

SDSS-IV MANGA: VARIATION OF THE STELLAR INITIAL MASS FUNCTION IN SPIRAL AND EARLY-TYPE GALAXIES

HONGYU LI^{1,2}, JUNQIANG GE¹, SHUDE MAO^{3,1,4}, MICHELE CAPPELLARI⁵, R. J. LONG^{1,4}, RAN LI^{1,6}, ERIC EMMELLEM^{7,8}, AARON A. DUTTON⁹, CHENG LI^{10,3}, KEVIN BUNDY¹¹, DANIEL THOMAS¹², NIV DRORY¹³, AND ALEXANDRE ROMAN LOPES¹⁴

Draft version March 16, 2017

ABSTRACT

We perform Jeans anisotropic modeling (JAM) on elliptical and spiral galaxies from the MaNGA DR13 sample. By comparing the stellar mass-to-light ratios estimated from stellar population synthesis (SPS) and from JAM, we find a similar systematic variation of the initial mass function (IMF) as in the earlier ATLAS^{3D} results. Early type galaxies (elliptical and lenticular) with lower velocity dispersions within one effective radius are consistent with a Chabrier-like IMF while galaxies with higher velocity dispersions are consistent with a more bottom heavy IMF such as the Salpeter IMF. Spiral galaxies have similar systematic IMF variations, but with slightly different slopes and larger scatters, due to the uncertainties caused by higher gas fractions and extinctions for these galaxies. Furthermore, we examine the effects of stellar mass-to-light ratio gradients on our JAM modeling, and find that the trends from our results becomes stronger after considering the gradients.

Subject headings: dark matter — galaxies: evolution — galaxies: formation — galaxies: kinematics and dynamics — galaxies: structure

1. INTRODUCTION

Stellar mass is one of the fundamental attributes of a galaxy. Accurate estimation of stellar mass plays an important role in the study of a galaxy’s structure, evolution and formation (Cappellari 2016). Stellar population synthesis (SPS) is the most popular method for obtaining the stellar mass. However, the stellar mass so obtained depends strongly on assuming a stellar initial mass func-

tion (IMF). Estimated stellar masses will shift on average 0.25 dex higher by changing the IMF from the Chabrier IMF (Chabrier 2003) to the Salpeter IMF (Salpeter 1955) (see Panter et al. 2007; Tortora et al. 2009). This causes uncertainty in the determination of the dark matter fraction in a galaxy’s central region (Cappellari et al. 2006; Tortora et al. 2009). Furthermore, whether the IMF is universal or not has been discussed for decades (Bastian, Covey, & Meyer 2010). The situation is becoming clearer after numerous studies based on line-strength indices (e.g. Conroy & van Dokkum 2012; Spiniello et al. 2012), strong lensing plus spatially unresolved stellar kinematics (e.g. Treu et al. 2010; Posacki et al. 2015), resolved stellar kinematics (Cappellari et al. 2012, 2013a), and the fundamental plane (Dutton et al. 2013a). All these studies show evidence for variation of the IMF in early type (i.e. elliptical or lenticular) galaxies.

In Cappellari et al. (2012), the Jeans anisotropic modeling technique (JAM, Cappellari 2008) was used, with a spatially constant stellar mass-to-light ratio and several different dark matter halo models, to obtain stellar mass estimates without resorting to SPS. They used 256 early type galaxies from the ATLAS^{3D} integral field unit (IFU) survey, and found a systematic variation in the IMF with galaxy stellar mass-to-light ratio. With the increasing availability of IFUs, more and more nearby galaxies with IFU data are becoming available, e.g. CALIFA (Sánchez et al. 2012), SAMI (Bryant et al. 2015) and MaNGA (Bundy et al. 2015). The MaNGA DR13 (SDSS Collaboration et al. 2016) sample includes 1390 galaxies of different morphologies (both early and late type galaxies), and is currently the largest IFU sample. Please see the following references for more details about the MaNGA instrumentation (Drory et al. 2015), observing strategy (Law et al. 2015), spectrophotometric calibration (Smee et al. 2013; Yan et al. 2016a), and survey execution and initial data quality (Yan et al. 2016b). In

¹ National Astronomical Observatories, Chinese Academy of Sciences, 20A Datun Road, Chaoyang District, Beijing 100012, China (hyli@nao.cas.cn)

² University of Chinese Academy of Sciences, Beijing 100049, China

³ Physics Department and Tsinghua Centre for Astrophysics, Tsinghua University, Beijing 100084, China

⁴ Jodrell Bank Centre for Astrophysics, School of Physics and Astronomy, The University of Manchester, Oxford Road, Manchester M13 9PL, UK

⁵ Sub-Department of Astrophysics, Department of Physics, University of Oxford, Denys Wilkinson Building, Keble Road, Oxford, OX1 3RH, UK

⁶ Key laboratory for Computational Astrophysics, National Astronomical Observatories, Chinese Academy of Sciences, Beijing, 100012, China

⁷ Université Lyon 1, Observatoire de Lyon, Centre de Recherche Astrophysique de Lyon and Ecole Normale Supérieure de Lyon, 9 avenue Charles André, F-69230 Saint-Genis Laval, France

⁸ European Southern Observatory, Karl-Schwarzschild-Str. 2, 85748 Garching, Germany

⁹ New York University Abu Dhabi, PO Box 129188, Abu Dhabi, UAE

¹⁰ Shanghai Astronomical Observatory, Shanghai 200030, China

¹¹ Kavli IPMU (WPI), UTIAS, The University of Tokyo, Kashiwa, Chiba 277-8583, Japan

¹² Institute of Cosmology & Gravitation, University of Portsmouth, Dennis Sciama Building, Portsmouth, PO1 3FX, UK

¹³ McDonald Observatory, The University of Texas at Austin, 1 University Station, Austin, TX 78712, USA

¹⁴ Department of Physics and Astronomy, Universidad de La Serena, Cisternas 1200, La Serena, Chile

this paper, we take advantage of the MaNGA DR13 sample to investigate IMF variation for both early type and late type galaxies using a similar method to Cappellari et al. (2012). Furthermore, we examine the effects of stellar mass-to-light ratio gradients (Portinari & Salucci 2010; Tortora et al. 2011; Ge et al., in preparation) on our dynamical models (i.e. not using a constant stellar mass-to-light ratio).

The structure of this paper is as follows. In Section 2, we briefly introduce the galaxy sample and the modeling methods we use. In Section 3, we show our results concerning the systematic variation of the IMF, and the effects of stellar mass-to-light ratio gradients. In Section 4, we summarize and give our conclusions.

2. MANGA SAMPLE AND METHODS

2.1. MaNGA sample

We use the MaNGA Product Launch 4 (MPL4) IFU spectra from the MaNGA DR13 SDSS-IV sample. The IFU spectra are extracted using the official data reduction pipeline (DRP, Law et al. 2016) and kinematical data are extracted using the official data analysis pipeline (DAP, Westfall et al. in prep). From the 1390 galaxies in the MaNGA DR13 catalogue, we exclude merging galaxies (close galaxy pairs, extremely unsmooth structures) and galaxies with low data quality (with less than 20 Voronoi bins with S/N greater than 30). In total, we are left with 816 galaxies (413 spiral galaxies; 403 elliptical and lenticular galaxies), more than a factor of three times larger than the ATLAS^{3D} sample. We visually select galaxies with the best data qualities and JAM modeling as our class A subsample (sufficient Voronoi bins, high S/N, no strong bars and spiral arms – these galaxies will have reliable JAM models). There are 346 galaxies in the class A subsample. We match our whole galaxy sample with *Galaxy Zoo 1* (Lintott et al. 2008) to obtain galaxy morphologies.

2.2. Stellar population synthesis

To assess the robustness of our results, we derive the stellar masses of all our galaxies using two different full spectrum fitting software and two different SPS template libraries. In both software packages we adopted for reference a Salpeter (1955) IMF. The first stellar mass estimate uses the **STARLIGHT** software (Cid Fernandes et al. 2005), in combination with the BC03 SPS templates (Bruzual & Charlot 2003), while the second uses the **pPXF** software (Cappellari & Emsellem 2004; Cappellari 2017) with the MILES-based (Sánchez-Blázquez et al. 2006) SPS models of Vazdekis et al. (2010). For **STARLIGHT**, we use 25 ages ($\log \text{Age} = [6.00, 6.50, 6.70, 6.82, 6.94, 7.00, 7.16, 7.40, 7.60, 7.74, 8.01, 8.21, 8.46, 8.71, 8.96, 9.11, 9.16, 9.40, 9.63, 9.80, 9.88, 10.00, 10.11, 10.18, 10.26]$ years), and 6 metallicities ($[\text{Z}/\text{H}] = [-1.7, -1.3, -0.7, -0.4, 0.0, 0.4]$). For **pPXF**, we use 25 ages linearly-spaced in $\log \text{Age}$ (yr) between 7.8 and 10.25, and 6 metallicities ($[\text{Z}/\text{H}] = [-1.7, -1.3, -0.7, -0.4, 0.0, 0.2]$). As can be seen from Fig. 1, the stellar mass-to-light ratios obtained from different templates and software agree well for galaxies with higher stellar mass-to-light ratios (i.e. old ages). The scatter is less than 0.1 dex and with nearly no bias. For galaxies with lower stellar mass-to-light ratios (i.e. young ages), **pPXF** with MILES tem-

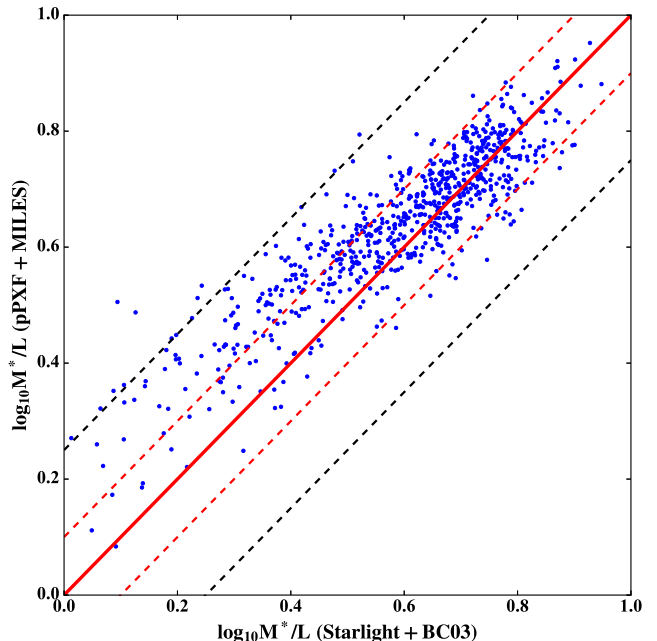


FIG. 1.— Comparison of the stellar mass-to-light ratios for all 816 galaxies between the **pPXF** software with MILES templates and the **STARLIGHT** software with BC03 templates. The red dashed lines show a 0.1 dex difference, and the black dashed lines show a 0.25 dex difference, which is the difference between the Salpeter and Chabrier IMFs.

plates gives systematically higher stellar mass-to-light ratios than **STARLIGHT** with BC03. This is because the M^*/L is more degenerate for younger galaxies than for older ones. The reason for this is that in young galaxies the light of few bright stars can dominate the flux in a galaxy’s spectrum. This makes it easy to ‘hide’ significant numbers of old stars, which emit a small amount of light, but contribute significantly to the mass, increasing the M^*/L . However, the difference between Salpeter and Chabrier IMF is 0.25 dex, so this 0.1 dex difference will not strongly affect our conclusions. This is shown explicitly in Section 3.1, where consistent IMF trends are presented using stellar masses from both **STARLIGHT** and **pPXF**. We use 0.1 dex as the uncertainty in the SPS in the following analysis. More details about the comparison of software packages and templates can be found in Ge et al. (in preparation).

We calculate our stellar mass-to-light ratios using Equation 2 in Cappellari et al. (2013a)

$$(M^*/L)_{\text{SPS}} = \frac{\sum_{j=1}^N w_j M_j^{\text{nogas}}}{\sum_{j=1}^N w_j L_j}, \quad (1)$$

where M_j^{nogas} is the stellar mass of the j th template, which includes the mass in living stars and stellar remnants, but excludes the gas lost during stellar evolution. L_j is the corresponding r-band luminosity. w_j is the weight of the j th template.

Before spectrum fitting, the data cubes are Voronoi binned (Cappellari & Copin 2003) to a S/N=30. For all resulting Voronoi bins in each galaxy, the two software fit for both the templates weights and for the dust extinction, adopting a Calzetti et al. (2000) reddening curve. The luminosity of each spatial bin is separately corrected for the measured extinction, before comput-

ing the total r-band $(M^*/L)_{\text{SPS}}$ for a galaxy by summing the luminosity and masses of all the bins within the MaNGA field-of-view. This dust extinction corrected $(M^*/L)_{\text{SPS}}$ is directly comparable with the stellar mass-to-light ratios in JAM modeling, obtained from stellar masses divided by the observed r-band luminosities. See Section 3.3 for more discussion about the extinction and inclination effects.

2.3. Dynamical modeling

We perform Jeans Anisotropic Modeling (JAM, Cappellari 2008) for all 816 selected galaxies. For a given luminosity density (constructed by fitting a galaxy’s surface brightness using `mge_fit_sectors` software (Cappellari 2002) and deprojecting it using the Multi-Gaussian Expansion (MGE) method of Emsellem, Monnet, & Bacon 1994), we assume a spatially constant stellar mass-to-light ratio and a gNFW dark halo profile (also see Barnabè et al. 2012; Cappellari et al. 2013a)

$$\rho_{\text{DM}}(r) = \rho_s \left(\frac{r}{R_s} \right)^\gamma \left(\frac{1}{2} + \frac{1}{2} \frac{r}{R_s} \right)^{-\gamma-3} \quad (2)$$

to construct a galaxy’s total mass model. From running JAM within an MCMC framework (`emcee`, Foreman-Mackey et al. 2013), we find the best-fitting parameters (including the stellar mass-to-light ratio $(M^*/L)_{\text{JAM}}$) which give the best model matching the galaxy’s observed second velocity moment map. We correct the cosmological surface brightness dimming effect in our MGE by multiplying the surface brightness by a factor $(1+z)^3$, which accounts both for the bolometric surface brightness dimming and the change of the band width (in the AB system). Since the MaNGA galaxies are mostly of low redshift (median and maximum redshift of the MaNGA sample are 0.03 and 0.15 respectively), we choose not to apply K-correction (e.g. Hogg et al. 2002) here. The stellar mass-to-light ratios obtained from this method are independent of SPS, and so can be used to test the variation of the IMF. The details of the modeling process are described in Li et al. (2016), which assesses the validity of the JAM method using cosmologically simulated galaxies. We broaden the prior for the central dark halo slope γ from $[-1.2, 0]$ to $[-1.6, 0]$ to avoid the bias in the IMF, which is sensitive to the halo response to baryonic settling (Dutton et al. 2013a). The prior is consistent with simulated haloes in the EA-GLE cosmological simulation (Schaller et al. 2015), as well as elliptical galaxy zoom-in simulations which find inner slopes of ~ -1.6 (Dutton et al. 2015), and spiral galaxies simulations which can have inner slopes of ~ 0 (Tollet et al. 2016).

Since spiral galaxies have higher gas fractions, especially later type spirals (Combes et al. 2013; Jaskot et al. 2015; Huang et al. 2012), we need to consider the gas contribution to the stellar masses derived from JAM. We perform the following steps to reduce the effects of cold gas in spiral galaxies:

1. We use the $M^{\text{gas}}-M^*$ relation from (Huang et al. 2012, Equation 1) to estimate the gas mass for every spiral galaxy. The stellar masses we use in applying the Huang relationship are taken from SPS.
2. We assume the gas ($\text{HI} + \text{H}_2$) mass distribution

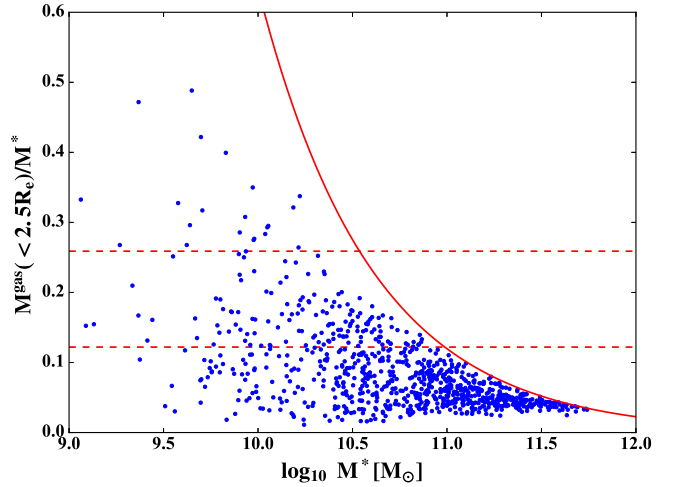


FIG. 2.— Gas mass fraction for all the spiral galaxies. The red solid line shows the gas fraction for a given stellar mass if all the gas is within $2.5R_e$. The red dashed lines show the fraction at which the M^*/L_{JAM} will change by 0.05 dex and 0.1 dex in the gas correction respectively.

can be approximated by an exponential disk with scale length 6.1 kpc (Bigiel & Blitz 2012).

3. We calculate the gas mass within $2.5R_e$ for every spiral galaxy using the gas mass profile described above.
4. We use the formula below to correct for the effect of gas in the JAM stellar mass-to-light ratios for spiral galaxies

$$(M^*/L)_{\text{JAM}}^{\text{nogas}} = \frac{M_{\text{JAM}}^* - M^{\text{gas}}(< 2.5R_e)}{L}, \quad (3)$$

where $(M^*/L)_{\text{JAM}}^{\text{nogas}}$ is the final value that we use to investigate IMFs, M_{JAM}^* is the stellar mass estimated by JAM, and $M^{\text{gas}}(< 2.5R_e)$ is the gas mass within $2.5R_e$.

In Fig. 2, we plot the gas mass fraction within $2.5R_e$ vs. galaxy stellar mass to show the impact of the gas correction. As can be seen, for massive spiral galaxies ($\log M^* > 11.0$), the gas fraction is smaller than 10%, which has nearly no effect on the dynamical models. As shown by the red dashed lines, the change of $(M^*/L)_{\text{JAM}}$ is smaller than 0.05 dex for more than half of the galaxies, and smaller than 0.1 dex for more than 90% of the galaxies.

3. RESULTS

In this section, we first show the systematic variation of the IMF and make a comparison with ATLAS^{3D} results. We then show the results from including the stellar mass-to-light ratio gradients.

3.1. Systematic variation of IMF

In order to describe the variation of the IMF, we define the IMF mismatch parameter similar to Treu et al. (2010)

$$\alpha_{\text{IMF}} \equiv (M^*/L)_{\text{JAM}}^{\text{nogas}} / (M^*/L)_{\text{SPS}}, \quad (4)$$

where α_{IMF} is the ratio of the M^*/L values obtained by JAM and SPS for a Salpeter IMF. In Fig. 3, we plot the

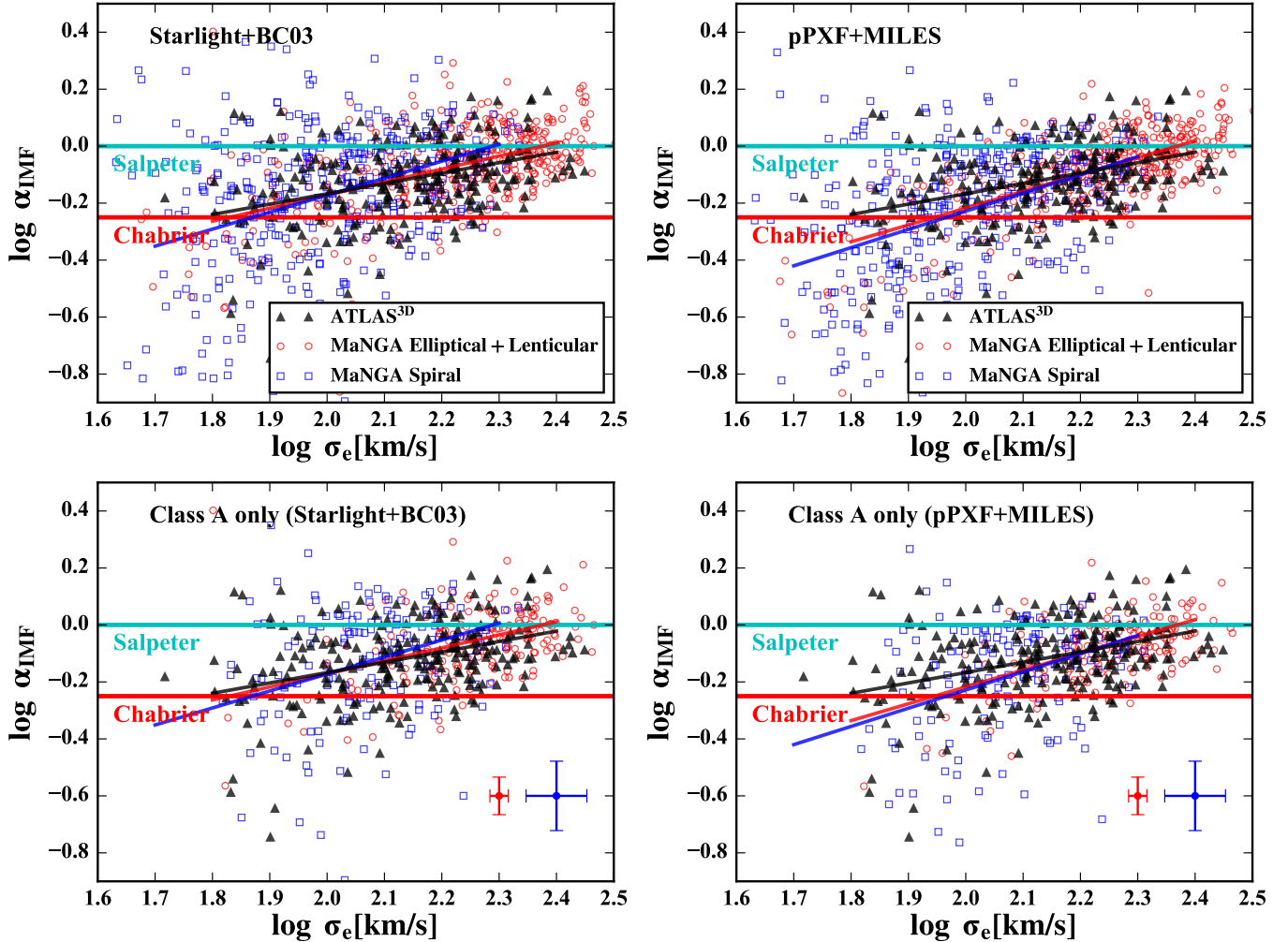


FIG. 3.— Systematic IMF variation for MaNGA galaxies. Upper left: the $\log \alpha_{\text{IMF}}$ for **STARLIGHT** + BC03 vs. galaxy velocity dispersion. Lower left: class A sample only, which has the most reliable fitting among the whole sample. Upper right: the $\log \alpha_{\text{IMF}}$ for **pPXF** + MILES vs. galaxy velocity dispersion. Lower right: class A sample only. In each panel, the black triangles show the results from ATLAS^{3D}, red circles for the MaNGA elliptical galaxies and blue squares for MaNGA spiral galaxies. The solid lines show the linear fitting results respectively. The horizontal colored solid lines show the positions where the stellar mass-to-light ratios from JAM equal the SPS with a Salpeter IMF (cyan) and SPS with a Chabrier IMF (red). The mean errors for elliptical and spiral galaxies are shown in the red and blue error bars in the lower panels respectively. The error in $(M^*/L)_{\text{JAM}}$ is estimated using the MCMC 1D marginalised distribution, while the error in $(M^*/L)_{\text{SPS}}$ is obtained by using different stellar templates and software in SPS.

mismatch parameter α_{IMF} vs. the velocity dispersion within an effective radius. The left panels are for the results from **STARLIGHT** + BC03, while the right panels are for the results from **pPXF** + MILES. The velocity dispersion is defined as

$$\sigma_e = \sqrt{\langle v_{\text{los}}^2(< R_e) \rangle}, \quad (5)$$

with $v_{\text{los}}^2 \equiv V^2 + \sigma^2$, where V and σ are the mean velocity and dispersion of the Gaussian which best fits the line-of-sight velocity distribution. A parameter value of $\alpha_{\text{IMF}} = 1$ means that JAM and SPS give the same estimate.

As can be seen from the panels, α_{IMF} changes systematically with velocity dispersion. Galaxies with higher velocity dispersions are consistent with a Salpeter IMF, while galaxies with lower velocity dispersions are consistent with a Chabrier IMF. This is true for both elliptical and spiral galaxies, although there are larger scatters for spiral galaxies due to the effects from cold gas, dust extinction and larger degeneracies between dark matter

and stellar mass.

We compare the systematic variation between different SPS software packages and templates in the left and right panels (left for **STARLIGHT**+BC03, right for **pPXF**+ MILES). As can be seen, there are some small differences between the two approaches, however the trends are consistent within the statistical errors as quantified in Table 1. The small differences can be understood as being due to the residual systematic differences between the two approaches, illustrated in Fig. 1. We fit the trend using a linear relation

$$\log \alpha_{\text{IMF}} = a + b \times \log \sigma_e \quad (6)$$

The fitting results are listed in Table 1 and plotted in Fig. 3.

The scatter for spiral galaxies with lower velocity dispersions is large since they are more affected by cold gas and dust extinction. The degeneracy between dark matter and stellar mass for these galaxies is also larger. There are some outliers with low velocity dispersion but

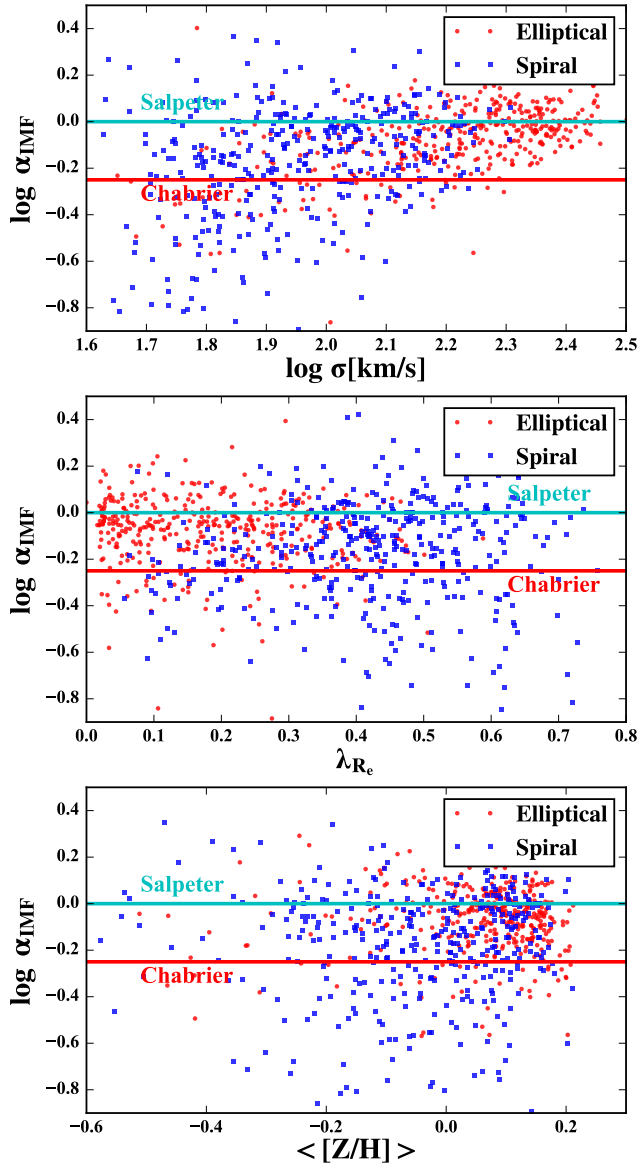


FIG. 4.— $\log \alpha_{\text{IMF}}$ vs. $\log \sigma$ (top), λ_{R_e} (middle) and metallicity (bottom). Other labels and legends are the same as Fig. 3.

TABLE 1
THE FITTING COEFFICIENTS OF $\log \sigma_e$ - $\log \alpha$ RELATION
(EQUATION 6) FOR ELLIPTICAL AND SPIRAL GALAXIES

	a	b	Δ_{int}
MaNGA elliptical (STARLIGHT)	-1.086 ± 0.006	0.457 ± 0.033	0.082
MaNGA elliptical (pPXF)	-1.399 ± 0.005	0.591 ± 0.030	0.063
MaNGA spiral (STARLIGHT)	-1.364 ± 0.011	0.596 ± 0.069	0.156
MaNGA spiral (pPXF)	-1.506 ± 0.011	0.638 ± 0.075	0.173
ATLAS ^{3D}	-0.895 ± 0.009	0.364 ± 0.042	0.083

Notes: The units of $\log \sigma_e$ in the fitting are km/s. Δ_{int} is the intrinsic scatter. The fitting is performed using the `ItsLinefit` software from Cappellari et al. (2013b).

high α_{IMF} . We check the JAM and SPS model fitting results for these galaxies, and find that they are galaxies with poor data quality (large uncertainties in dynamical modelling and SPS) or high inclination (edge-on galaxies, strong dust extinction). Our results are also consistent with results from gravitational lensing, albeit at slightly higher redshift $z = 0.2$ (Treu et al. 2010). However, there are also a few discordant cases in Smith & Lucey (2013) and Smith et al. (2015). In order to demonstrate that the IMF trend is not caused by the poor data quality of some galaxies, we plot these trends using the class A subsample only in the lower panels of Fig. 3, which have the most reliable fitting among the whole sample.

In addition to σ_e (cf. eq. 5), which approximates the true projected velocity second moment, and includes contribution from both ordered rotation V and random motion σ , we also check whether α_{IMF} depends on σ alone, with the ordered rotation contribution removed. We additionally check the dependence against the specific stellar angular momentum parameter λ_{R_e} (Emsellem et al. 2007) and metallicity $[Z/H]$. σ is defined as

$$\sigma = \sqrt{\langle \sigma_{\text{los}}^2(< R_e) \rangle}, \quad (7)$$

which removes the velocity term in σ_e . The results are shown in Fig. 4. The IMF trend is similar after changing σ_e to σ . For λ_{R_e} and metallicity $[Z/H]$, there is no significant correlation with α_{IMF} . This is similar to results from McDermid et al. (2014), who found no strong correlation between IMF and metallicity using the same JAM modeling method. Martín-Navarro et al. (2015), however, using line indices, showed that there is a correlation. This could be due to differences between the two methods.

More results about dark matter fractions, and the fundamental plane, stellar mass plane and mass plane scaling relationships will be given in a following paper (Li et al., in preparation).

3.2. Effects of the stellar mass-to-light ratio gradient

For simplicity, when constructing mass models in JAM, a constant stellar mass-to-light ratio is usually assumed in order to convert a luminosity distribution to a stellar mass distribution, e.g. in Cappellari et al. (2013b). Only recently have dynamical models started to include spatial variations in the stellar mass-to-light ratio, in addition to allowing for a dark matter component (Mitzkus, Cappellari, & Walcher 2017; Poci, Cappellari, & McDermid 2016). This can be important, as a galaxy’s stellar population may not be spatially uniform, so there may be a stellar mass-to-light ratio gradient, especially for younger galaxies (Portinari & Salucci 2010; Tortora et al. 2011; Ge et al., in preparation). In addition, different dust extinction levels at different radii may also affect the mass-to-light ratio profile. It is important therefore to examine the effects caused by mass-to-light ratio gradients.

In order to test the effects of such a gradient, we use the stellar mass profile directly in our mass models instead of the luminosity profile. In doing so, we avoid the assumption of a constant stellar mass-to-light ratio. The stellar mass profile is determined using our full spectrum fitting approach from the MaNGA spectra as described

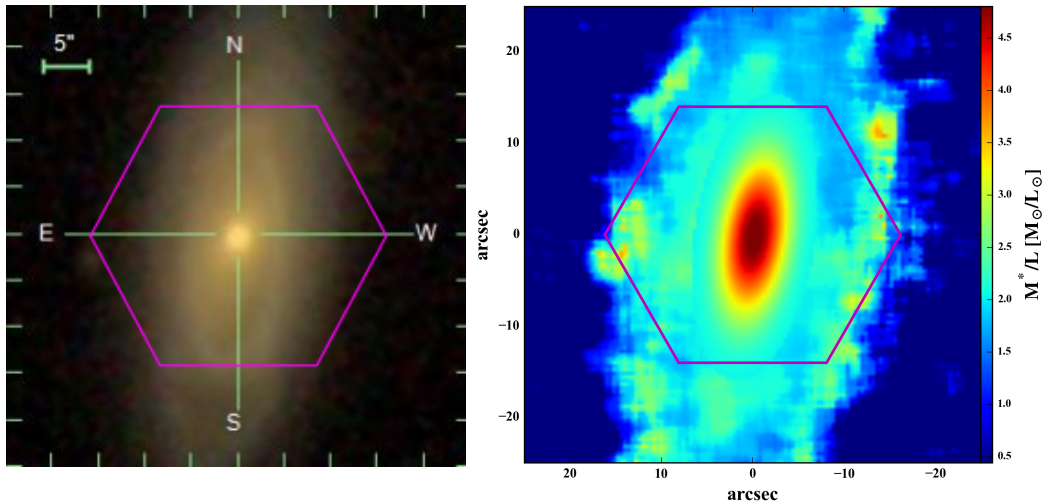


FIG. 5.— The galaxy’s SDSS 3-color image (left) and stellar mass-to-light ratio map (right). The magenta hexagon shows the region where IFU data are available. The inner stellar mass-to-light ratios are from MaNGA spectra and the outer are estimated by color map.

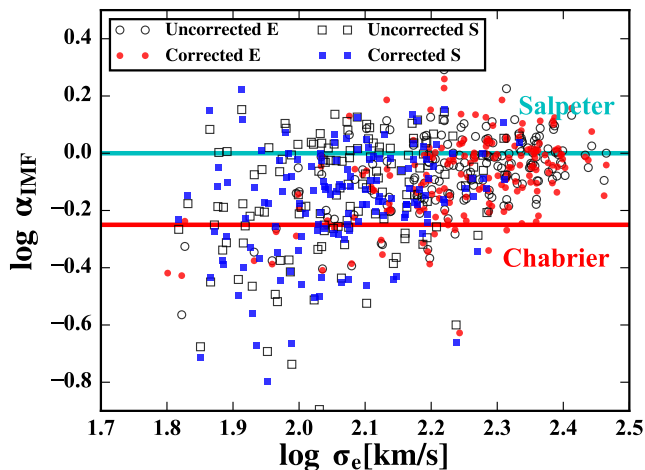


FIG. 6.— $\log \alpha_{\text{IMF}}$ vs. $\log \sigma_e$ for class A galaxies with the stellar mass-to-light ratio gradient correction applied. The black void circles and squares show the positions of the galaxies without correction for elliptical and spiral galaxies respectively, the red circles and blue squares show the positions after correction. Other labels and legends are the same as Fig. 3.

in Section 2.2. The spectra and kinematics are, by design, available over the same region. This is the spatial region where the models are fitted and consequently is the region for which we can constrain the density profiles. The results of dynamical models are only weakly dependent on the adopted stellar mass profiles at larger radii (Krajnović et al. 2005). For this reason, the determination of accurate stellar mass profiles only really matters within the MaNGA field of view. However, to avoid an abrupt and unphysical discontinuity in the stellar mass profile, outside the edge of the MaNGA field of view, we use the more approximate color- M^*/L relation to smoothly extend the profile out to larger radii.

In practice, to estimate the stellar mass density for our models, we start from the r-band image and multiply the surface brightness of each pixel contained within the MaNGA field of view by the stellar mass-to-light ratios measured from spectral fitting to obtain a stellar mass

surface density map. At larger radii we estimate the stellar mass-to-light ratios from galaxy’s color. We take the SDSS g band and i band images (Gunn et al. 2006; Eisenstein et al. 2011) and calculate the $g-i$ color in each pixel. We apply the color- M^*/L relationship from Bell et al. (2003) to convert the color to the stellar mass-to-light ratio. We assume a Salpeter IMF in the conversion. We use a median filter with window size 9 by 9 pixels (empirically chosen) to obtain a smoothed map. We scale the normalisation of the outer part to match the $(M^*/L)_{\text{SPS}}$ values of the inner part around 1Re. This is to avoid a discontinuity in the profile, although the scale factor is near 1 for majority of the galaxies. After obtaining the stellar mass surface density map, we perform the MGE fitting to it to obtain a stellar mass MGE. We then use this stellar mass MGE in our mass model (the luminous MGE is still used as tracer density in JAM modeling). Since we already use stellar mass distribution in the mass model, the scale factor parameter in JAM is not M^*/L any more, but the mismatch parameter α_{IMF} instead.

In Fig. 5, we show one galaxy as an example (MaNGA plate-IFU design : 8313-12705) which has one of the largest stellar mass-to-light ratio gradients in our galaxy sample. As can be seen from the color map in the right panel of Fig. 5, the stellar mass-to-light ratio at the galaxy center is ~ 5.0 , decreasing to ~ 2.0 in the outer regions.

We take Class A subset of galaxies and rerun JAM modeling with the gradient correction applied. In Fig. 6, we plot the IMF mismatch parameter α_{IMF} vs. $\log \sigma_e$ as in Fig. 3 for these galaxies. As can be seen in the figure, even though there is some scatter after applying the gradient correction, the systematic variation still exists, and in fact it becomes even stronger.

In Fig. 7, we plot the change of mismatch parameter ($\Delta \log \alpha_{\text{IMF}} = \log \alpha_{\text{IMF}}^{\text{corrected}} - \log \alpha_{\text{IMF}}^{\text{uncorrected}}$) vs. $\Delta_{M^*/L}$ and $\log \sigma_e$. $\Delta_{M^*/L}$ is the stellar mass-to-light ratio gradient obtained by fitting the linear function $\log M^*/L = a + b \log R$ to the MaNGA IFU results. As can be seen in the top panel, the change in the mismatch parameter increases as the gradient becomes larger (more negative).

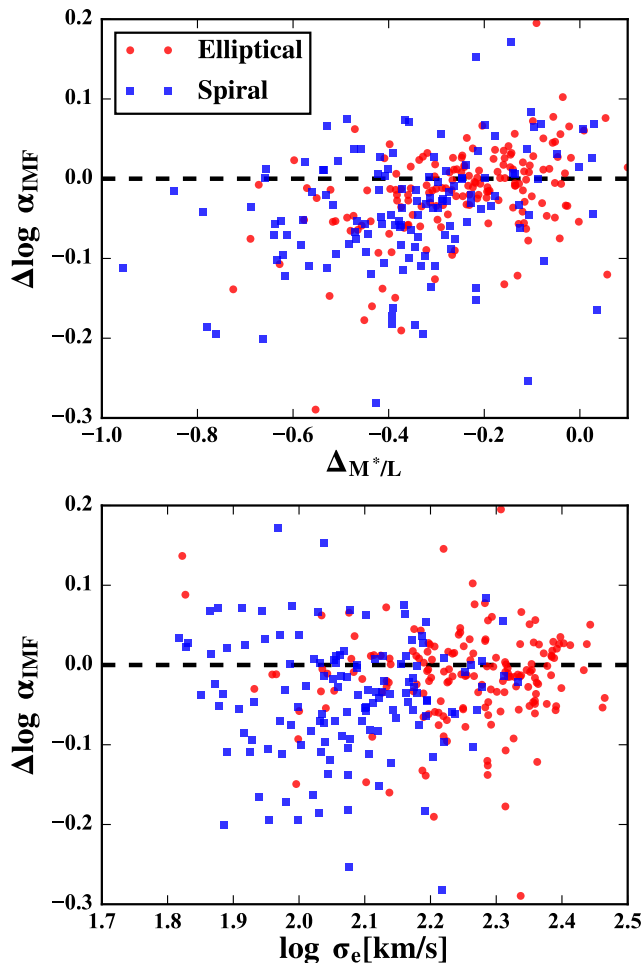


FIG. 7.— Change of the mismatch parameter ($\Delta \log \alpha_{\text{IMF}} = \log \alpha_{\text{IMF}}^{\text{corrected}} - \log \alpha_{\text{IMF}}^{\text{uncorrected}}$) vs. gradient (upper) and velocity dispersion (lower). The red circles are elliptical galaxies and blue squares are spiral galaxies.

When the gradient is close to 0, the α_{IMF} before and after correction has no systematic difference. However when the gradient increases, α_{IMF} systematically decreases after gradient correction (implying lighter IMFs). In the lower panel, one can see that galaxies with lower velocity dispersions have systematically smaller α_{IMF} after the gradient correction (this means the systematic IMF trend become stronger after correcting for the gradient effect). This is because lower dispersion galaxies have younger stellar populations and steeper gradients. Our test suggests that the IMF trend is even stronger than what we determined for the case without gradients as well as in previously published studies.

3.3. Effect of inclination and dust extinction for spiral galaxy

In this section, we discuss the effects of inclination and dust extinction on spiral galaxies. Since observations suffer more from dust extinction when galaxies are nearly edge-on, the dynamical M/L of flat galaxies tends to be overestimated when galaxies are nearly face-on (Lablanche et al. 2012).

In the top and middle panels of Fig. 8, we show $\log \alpha_{\text{IMF}}$ vs. $\log \sigma_e$ for all the spiral galaxies in our sample with different observed axis ratios (i.e. inclinations)

and dust extinction. As can be seen, edge-on galaxies or galaxies with higher dust extinction are slightly biased to higher α_{IMF} . This may be because SPS underestimates the dust extinction or the age of these galaxies, which leads to a lower $(M^*/L)_{\text{SPS}}$. For intermediate and low inclination/dust extinction galaxies, there is no systematic difference. In the bottom panel of Fig. 8, we show the value of extinction predicted by our **STARLIGHT** SPS fits vs. axis ratio (i.e. inclination). As expected, edge-on galaxies have more dust extinction, and our trend is similar to the results using optical and near infrared photometry data obtained by Devour & Bell (2016). In Fig 9, we further compare the M^*/L_{SPS} assuming a CAL extinction law in SPS with the M^*/L_{SPS} assuming a CCM (Cardelli, Clayton, & Mathis 1989) extinction law and find no significant difference.

4. CONCLUSIONS

We have performed JAM modeling for 816 galaxies, with good data quality, from the MaNGA DR13 sample, including both elliptical and spiral galaxies. We have compared the stellar mass-to-light ratios from SPS and JAM modeling, and find a systematic variation of the initial mass function for both elliptical and spiral galaxies. Galaxies with lower velocity dispersions within an effective radius are consistent with a Chabrier-like IMF, while galaxies with higher velocity dispersions are consistent with a more bottom heavy IMF like the Salpeter IMF. These results agree well with previous studies (e.g. Conroy & van Dokkum 2012; Dutton et al. 2013a; Cappellari et al. 2012, 2013a; Posacki et al. 2015).

In previous IMF studies using stellar dynamics or gravitational lensing, a constant stellar mass-to-light ratio was assumed. However, there are stellar mass-to-light ratio gradients especially for young galaxies. So, in addition, we have examined the effect of this gradient. We use our Class A galaxies to introduce this gradient and performed a comparison test. We found that the systematic IMF trend still exists, and becomes even stronger after the gradient correction. In addition to the stellar mass-to-light ratio gradient, there are also studies which showed that the IMF inside a galaxy could also be different (Martín-Navarro et al. 2015; La Barbera et al. 2016). In their studies, they found that for several early type galaxies, the IMF is bottom heavy in the central region, but bottom light in the outer region. This will lead to an even steeper stellar mass-to-light ratio gradient and have some effects on our results. However, the systematic IMF trend in this work is based on a globally averaged IMF for a galaxy. The IMF variation inside a galaxy is beyond the scope of this paper, but we will return to issue in a future work.

Spiral galaxies with lower velocity dispersions have results with large scatters. This is because they are more affected by cold gas and dust extinction. The degeneracy between dark matter and stellar mass is also stronger in these galaxies. Our results show that these galaxies favour a Chabrier-like IMF, and this is consistent with the results in Bershady et al. (2011); Dutton et al. (2011); Brewer et al. (2012). Galaxy inclinations do not have strong effects except for nearly edge-on galaxies (higher dust extinction leads to larger uncertainty in SPS).

Observationally it will be interesting to examine further whether there are differences in the IMF between

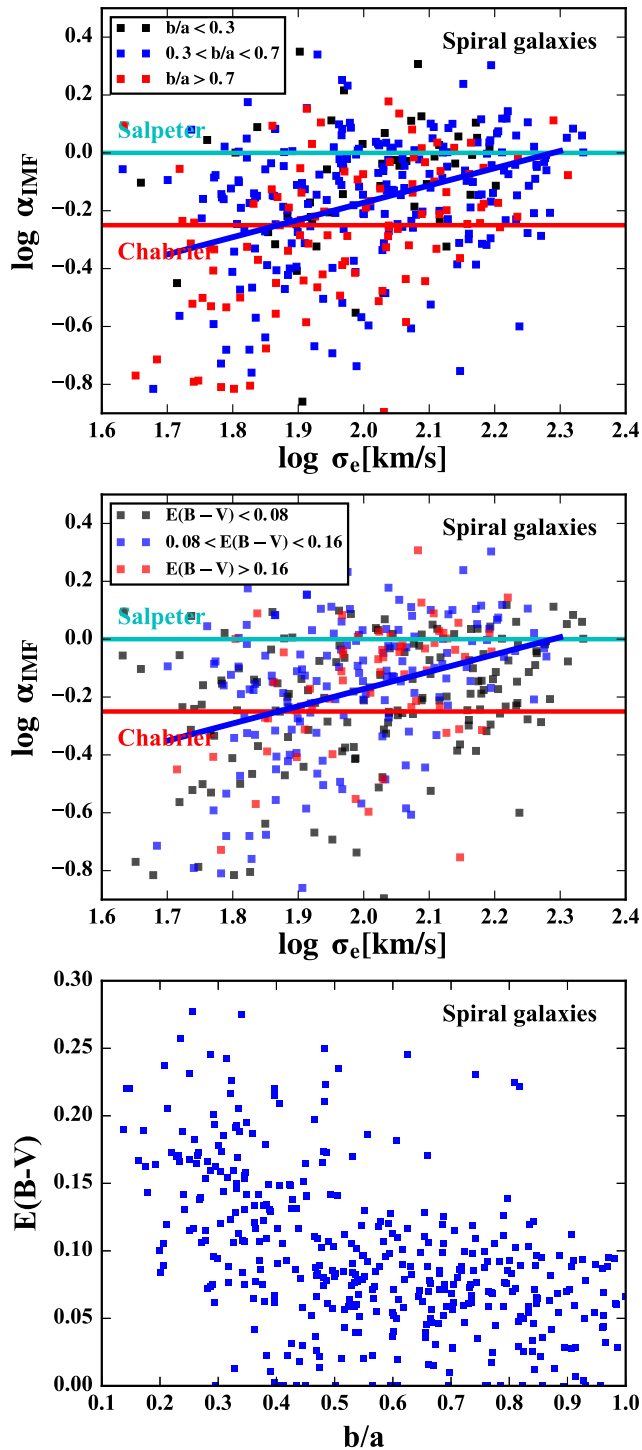


FIG. 8.— Top: $\log \alpha_{\text{IMF}}$ vs. $\log \sigma_e$ for all the spiral galaxies with different observed axis ratios. The black squares are for near edge-on sample ($b/a < 0.3$), blue squares for intermediate inclined sample ($0.3 < b/a < 0.7$) and red squares for near face-on sample ($b/a > 0.7$). The blue solid line shows the fitting results for spiral galaxies in Table 1. Middle: $\log \alpha_{\text{IMF}}$ vs. $\log \sigma_e$ for all the spiral galaxies with different extinction values predicted by SPS. The black squares are for low extinction sample ($E(B-V) < 0.08$), blue squares for intermediate extinction sample ($0.08 < E(B-V) < 0.16$) and red squares for high extinction sample ($E(B-V) > 0.16$). The blue solid line shows the fitting results for spiral galaxies in Table 1. Bottom: dust extinction values predicted by SPS (STARLIGHT) vs. observed axis ratios. Other labels are the same as Fig. 3.

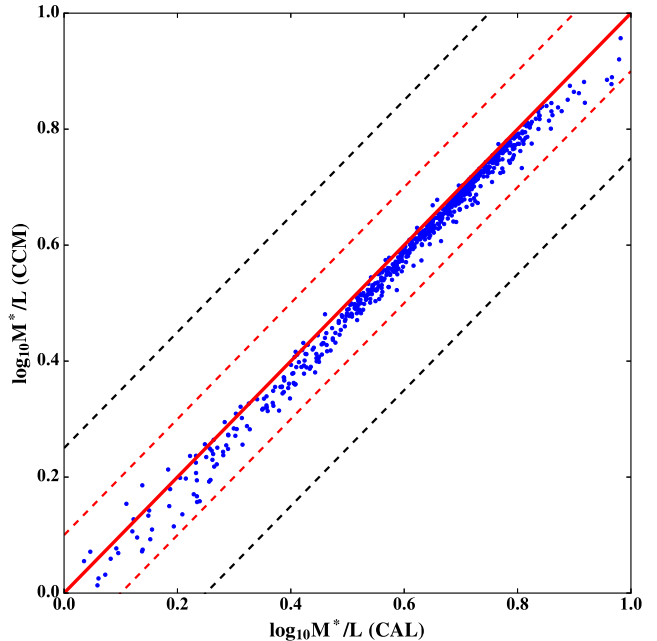


FIG. 9.— Comparison between the SPS stellar mass-to-light ratios determined using both the CAL and CCM extinction laws. The lines are the same as Fig. 1.

galaxy discs and bulges in spiral galaxies (e.g. Dutton et al. 2013b). Theoretically it is unclear how the IMF changes when two galaxies with different IMFs merge, and whether the IMF variation changes as a function of redshift. If it does, how this changes the stellar mass function of galaxies and the evolution of the stellar mass as a function of cosmic time needs investigation.

ACKNOWLEDGEMENTS

HL would like to thank Drs. Yiping Shu and Zheng Zheng for many useful discussions, and Drs. Anne Jaskot and David Stark for advice on the gas fraction for spiral galaxies. MC acknowledges support from a Royal Society University Research Fellowship. We performed our computer runs on the Zen high performance computer cluster of the National Astronomical Observatories, Chinese Academy of Sciences (NAOC). This work has been supported by the Strategic Priority Research Program “The Emergence of Cosmological Structures” of the Chinese Academy of Sciences Grant No. XDB09000000 (RJL and SM), and by the National Natural Science Foundation of China (NSFC) under grant numbers 11333003, 11390372 (SM), and 11303033, 11511130054, 11333001 (RL), by the Newton Fund, by the Youth Innovation Promotion Association of CAS, and by World Premier International Research Center Initiative (WPI Initiative), MEXT, Japan.

Funding for the Sloan Digital Sky Survey IV has been provided by the Alfred P. Sloan Foundation, the U.S. Department of Energy Office of Science, and the Participating Institutions. SDSS-IV acknowledges support and resources from the Center for High-Performance Computing at the University of Utah. The SDSS web site is www.sdss.org.

SDSS-IV is managed by the Astrophysical Research Consortium for the Participating Institutions of the SDSS Collaboration including the Brazilian Partici-

pation Group, the Carnegie Institution for Science, Carnegie Mellon University, the Chilean Participation Group, the French Participation Group, Harvard-Smithsonian Center for Astrophysics, Instituto de Astrofísica de Canarias, The Johns Hopkins University, Kavli Institute for the Physics and Mathematics of the Universe (IPMU) / University of Tokyo, Lawrence Berkeley National Laboratory, Leibniz Institut für Astrophysik Potsdam (AIP), Max-Planck-Institut für Astronomie (MPIA Heidelberg), Max-Planck-Institut für Astrophysik (MPA Garching), Max-Planck-Institut für

Extraterrestrische Physik (MPE), National Astronomical Observatories of China, New Mexico State University, New York University, University of Notre Dame, Observatório Nacional / MCTI, The Ohio State University, Pennsylvania State University, Shanghai Astronomical Observatory, United Kingdom Participation Group, Universidad Nacional Autónoma de México, University of Arizona, University of Colorado Boulder, University of Oxford, University of Portsmouth, University of Utah, University of Virginia, University of Washington, University of Wisconsin, Vanderbilt University, and Yale University.

REFERENCES

- Barnabè M., et al., 2012, *MNRAS*, 423, 1073
 Bastian N., Covey K. R., Meyer M. R., 2010, *ARA&A*, 48, 339
 Bell E. F., McIntosh D. H., Katz N., Weinberg M. D., 2003, *ApJS*, 149, 289
 Bershadsky M. A., Martinsson T. P. K., Verheijen M. A. W., Westfall K. B., Andersen D. R., Swaters R. A., 2011, *ApJ*, 739, L47
 Bigiel F., Blitz L., 2012, *ApJ*, 756, 183
 Brewer B. J., et al., 2012, *MNRAS*, 422, 3574
 Bruzual G., Charlot S., 2003, *MNRAS*, 344, 1000
 Bryant J. J., et al., 2015, *MNRAS*, 447, 2857
 Bundy K., et al., 2015, *ApJ*, 798, 7
 Calzetti D., Armus L., Bohlin R. C., Kinney A. L., Koornneef J., Storchi-Bergmann T., 2000, *ApJ*, 533, 682
 Cappellari M., 2002, *MNRAS*, 333, 400
 Cappellari M., Copin Y., 2003, *MNRAS*, 342, 345
 Cappellari M., Emsellem E., 2004, *PASP*, 116, 138
 Cappellari M., et al., 2006, *MNRAS*, 366, 1126
 Cappellari M., 2008, *MNRAS*, 390, 71
 Cappellari M., et al., 2012, *Natur*, 484, 485
 Cappellari M., et al., 2013a, *MNRAS*, 432, 1862
 Cappellari M., et al., 2013b, *MNRAS*, 432, 1709
 Cappellari M., 2016, *ARA&A*, 54, 597
 Cappellari M., 2017, *MNRAS*, 466, 798
 Cardelli J. A., Clayton G. C., Mathis J. S., 1989, *ApJ*, 345, 245
 Chabrier G., 2003, *PASP*, 115, 763
 Cid Fernandes R., Mateus A., Sodré L., Stasińska G., Gomes J. M., 2005, *MNRAS*, 358, 363
 Combes F., García-Burillo S., Braine J., Schinnerer E., Walter F., Colina L., 2013, *A&A*, 550, A41
 Conroy C., van Dokkum P. G., 2012, *ApJ*, 760, 71
 Devour B. M., Bell E. F., 2016, *MNRAS*, 459, 2054
 Drory N., et al., 2015, *AJ*, 149, 77
 Dutton A. A., et al., 2011, *MNRAS*, 416, 322
 Dutton A. A., Macciò A. V., Mendel J. T., Simard L., 2013, *MNRAS*, 432, 2496
 Dutton A. A., et al., 2013, *MNRAS*, 428, 3183
 Dutton A. A., Macciò A. V., Stinson G. S., Gutcke T. A., Penzo C., Buck T., 2015, *MNRAS*, 453, 2447
 Eisenstein D. J., et al., 2011, *AJ*, 142, 72
 Emsellem E., Monnet G., Bacon R., 1994, *A&A*, 285, 723
 Emsellem E., et al., 2007, *MNRAS*, 379, 401
 Foreman-Mackey D., Hogg D. W., Lang D., Goodman J., 2013, *PASP*, 125, 306
 Gunn J. E., et al., 2006, *AJ*, 131, 2332
 Hogg D. W., Baldry I. K., Blanton M. R., Eisenstein D. J., 2002, *astro*, arXiv:astro-ph/0210394
 Huang S., Haynes M. P., Giovanelli R., Brinchmann J., 2012, *ApJ*, 756, 113
 Jaskot A. E., Oey M. S., Salzer J. J., Van Sistine A., Bell E. F., Haynes M. P., 2015, *ApJ*, 808, 66
 Krajnović D., Cappellari M., Emsellem E., McDermid R. M., de Zeeuw P. T., 2005, *MNRAS*, 357, 1113
 La Barbera F., Vazdekis A., Ferreras I., Pasquali A., Cappellari M., Martín-Navarro I., Schönebeck F., Falcón-Barroso J., 2016, *MNRAS*, 457, 1468
 Lablanche P.-Y., et al., 2012, *MNRAS*, 424, 1495
 Law D. R., et al., 2015, *AJ*, 150, 19
 Law D. R., et al., 2016, *AJ*, 152, 83
 Li H., Li R., Mao S., Xu D., Long R. J., Emsellem E., 2016, *MNRAS*, 455, 3680
 Lintott C. J., et al., 2008, *MNRAS*, 389, 1179
 Martín-Navarro I., Barbera F. L., Vazdekis A., Falcón-Barroso J., Ferreras I., 2015, *MNRAS*, 447, 1033
 McDermid R. M., et al., 2014, *ApJ*, 792, L37
 Mitzkus M., Cappellari M., Walcher C. J., 2017, *MNRAS*, 464, 4789
 Panter B., Jimenez R., Heavens A. F., Charlot S., 2007, *MNRAS*, 378, 1550
 Poci A., Cappellari M., McDermid R. M., 2016, arXiv, arXiv:1612.05805
 Posacki S., Cappellari M., Treu T., Pellegrini S., Ciotti L., 2015, *MNRAS*, 446, 493
 Portinari L., Salucci P., 2010, *A&A*, 521, A82
 Salpeter E. E., 1955, *ApJ*, 121, 161
 Sánchez-Blázquez P., et al., 2006, *MNRAS*, 371, 703
 Schaller M., et al., 2015, *MNRAS*, 451, 1247
 Spiniello C., Trager S. C., Koopmans L. V. E., Chen Y. P., 2012, *ApJ*, 753, L32
 Sánchez S. F., et al., 2012, *A&A*, 538, A8
 SDSS Collaboration, et al., 2016, arXiv, arXiv:1608.02013
 Smee S. A., et al., 2013, *AJ*, 146, 32
 Smith R. J., Lucey J. R., 2013, *MNRAS*, 434, 1964
 Smith R. J., Alton P., Lucey J. R., Conroy C., Carter D., 2015, *MNRAS*, 454, L71
 Tortora C., Napolitano N. R., Romanowsky A. J., Capaccioli M., Covone G., 2009, *MNRAS*, 396, 1132
 Tortora C., Napolitano N. R., Romanowsky A. J., Jetzer P., Cardone V. F., Capaccioli M., 2011, *MNRAS*, 418, 1557
 Tollet E., et al., 2016, *MNRAS*, 456, 3542
 Treu T., Auger M. W., Koopmans L. V. E., Gavazzi R., Marshall P. J., Bolton A. S., 2010, *ApJ*, 709, 1195
 Vazdekis A., Sánchez-Blázquez P., Falcón-Barroso J., Cenarro A. J., Beasley M. A., Cardiel N., Gorgas J., Peletier R. F., 2010, *MNRAS*, 404, 1639
 Yan R., et al., 2016a, *AJ*, 151, 8
 Yan R., et al., 2016b, *AJ*, 152, 197